JACS
JOURNAL OF THE AMERICAN CHEMICAL SOCIETY
Article
pubs.acs.org/JACS

Unravelling Doping Effects on PEDOT at the Molecular Level: From Geometry to Thermoelectric Transport Properties

Wen Shi,[†] Tianqi Zhao,[†] Jinyang Xi,[†] Dong Wang,*[,†] and Zhigang Shuai*[,†,‡,§]

[†]MOE Key Laboratory of Organic OptoElectronics and Molecular Engineering, Department of Chemistry, Tsinghua University, Beijing 100084, PR China

[‡]Key Laboratory of Organic Solids, Beijing National Laboratory for Molecular Science (BNLMS), Institute of Chemistry, Chinese Academy of Sciences, Beijing 100190, PR China

[§]Collaborative Innovation Center of Chemistry for Energy Materials, Xiamen University, 351005 Xiamen, PR China

Supporting Information

ABSTRACT: Tuning carrier concentration via chemical doping is the most successful strategy to optimize the thermoelectric figure of merit. Nevertheless, how the dopants affect charge transport is not completely understood. Here we unravel the doping effects by explicitly including the scattering of charge carriers with dopants on thermoelectric properties of poly(3,4-ethylenedioxythiophene), PEDOT, which is a p-type thermoelectric material with the highest figure of merit reported. We corroborate that the PEDOT exhibits a distinct transition from the aromatic to quinoid-like structure of backbone, and a semiconductor-to-metal transition with an increase in the level of doping. We identify a close-to-unity charge transfer from PEDOT to the dopant, and find that the ionized impurity scattering dominates over the acoustic phonon scattering in the doped PEDOT. By incorporating both scattering mechanisms, the doped PEDOT exhibits mobility, Seebeck coefficient and power factors in very good agreement with the experimental data, and the lightly doped PEDOT exhibits thermoelectric properties superior to the heavily doped one. We reveal that the thermoelectric transport is highly anisotropic in ordered crystals, and suggest to utilize large power factors in the direction of polymer backbone and low lattice thermal conductivity in the stacking and lamellar directions, which is viable in chain-oriented amorphous nanofibers.

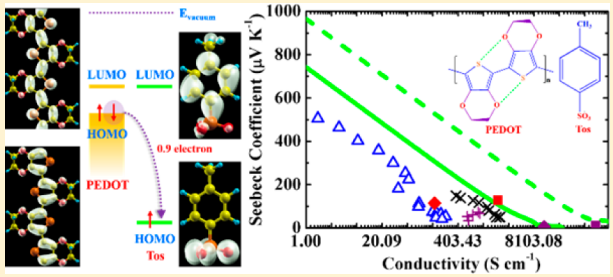

1. INTRODUCTION

Thermoelectric (TE) devices are one of the solid-state green energy solutions that utilize the TE materials to directly convert heat energy to electricity known as power generators, or electricity to temperature difference known as freezers.[1,2] The TE technology is particularly promising for powering human support on long manned missions during space flight. To compete with other clean energy solutions, highly efficient TE materials and devices are desired. The energy conversion efficiency of TE devices depends on an intrinsic material parameter known as the dimensionless TE figure of merit $zT = S^2\sigma T/\kappa$, in which S is the Seebeck coefficient, also known as the thermopower, σ is the electrical conductivity, T is the average absolute temperature of the hot and cold junctions, and κ is the thermal conductivity. In solids, both electrons and phonons are heat carriers, so the overall thermal conductivity is contributed by electrons as well as the lattice vibrations. The efficient TE materials are usually semiconductors, with high electrical conductivity, large thermopower, and low thermal conductivity. The optimization of TE efficiency is extremely challenging, because the electrical transport coefficients are interrelated and often contradict with each other. For example, the Seebeck coefficient usually decreases as the electrical conductivity increases. Engineering the electronic band structure and lattice thermal conductivity have been recognized as two effective strategies to improve the TE efficiency, which can be acquired simultaneously in one material.

Organic electronic materials are low-cost, easy to process, lightweight, and possess relatively low lattice thermal conductivity, making them advantageous over inorganic electronic materials for TE applications.[3−7] The first breakthrough is seen on PEDOT, where a zT of 0.25 was achieved through accurate control of the oxidation level with p-toluenesulfonate (Tos) as counterions,[8] and 0.42 was reported via the minimization of total dopant volume with poly(styrenesulfonate) (PSS) as counterions.[9] The optimized zT of PEDOT:PSS is 2 orders of magnitude higher than the nonoptimized one obtained in an early research.[10] Despite the experimental advance made, more up-to-date investigations point out that the measurement uncertainty in both Seebeck coefficient and thermal conductivity may cause overestimation of the zT value. For example, it has been shown that the transport properties of PEDOT samples are highly sensitive to the processing condition, so that an accurate zT value has to be obtained from measurements of the three transport properties

Received: June 30, 2015
Published: September 25, 2015

DOI: 10.1021/jacs.5b06584
J. Am. Chem. Soc. 2015, 137, 12929−12938

on exactly the same sample along the same direction.[11] Besides, it has been proposed that an inappropriate choice in the device geometry can lead to systematic errors in the measured value of Seebeck coefficient, by a factor of 3 or more.[12] Anyhow, tuning the carrier concentration via chemical doping has been demonstrated as one of the most successful strategies to maximize the performance of organic TE materials,[3,13] which decreases the Seebeck coefficient and increases the electrical conductivity simultaneously, resulting in a maximum of power factor at the optimal doping level. It is anticipated that the dopants mixed in the conducting polymers not only increase the carrier concentration, but also alter the configuration of the conducting host molecules, and influence their charge transport process. Because of inefficiency of the molecular doping, removing those dopants that make no contributions to doping has been shown to significantly enhance the TE efficiency.[9]

Density functional theory (DFT) investigations on the doping mechanism have been conducted for several organic semiconductors,[14−18] but the fundamental aspects underlying the doping effects on the ground state configuration, electronic structure and most importantly TE transport remain elusive at the molecular level for PEDOT. Inspired by the state-of-art experimental advances to optimize the TE figure of merit via the accurate control of doping level, in this work we uncover from first-principles the doping effects on the TE transport properties of PEDOT. To account for the doping effects, the counterions Tos have to be incorporated explicitly in the host model. As far as we have noticed, the explicit effect of doping on the TE transport properties, especially the scattering of charge carriers with the counterions, has never been explored before. Very recently, conducting polymers with excellent transport properties comparable or even superior to PEDOT have been reported.[19−24] we hope that our study on the doping control to improve the TE efficiency of PEDOT could stimulate more innovative research on conducting polymers as TE materials.

2. METHODS

2.1. Model Setup and Electronic Structure Calculations. In a real polymer thin film, both crystalline and amorphous domains present. As a first step, an ideal crystal model representing the crystalline domains is chosen. To mimic different levels of doping, two crystal models of doped PEDOT:Tos were set up with different amount of the Tos counterions in the unit cell. One is lightly doped PEDOT with eight EDOT moieties and one Tos in each unit cell, and the other is heavily doped PEDOT with eight EDOT moieties and two Tos in each unit cell. The eight EDOT are from four chains, each chain contributes two. It should be clarified that in the chemical model we choose the whole unit cell is kept neutral, and charge transfer between PEDOT and Tos occurs in the electronic structure calculations. The starting crystal structures of pristine and heavily doped PEDOT were taken directly from Jean-Luc Brédas's work,[18] in which refined structural models were built upon crystallographic data of PEDOT and other substituted polythiophenes. The lattice parameters and ionic positions of the starting structures were then optimized by the projector augmented wave (PAW) method with the Perdew−Burke−Ernzerhof including dispersion (PBE-D) exchange correlation functional in the Vienna ab initio simulation package (VASP, version 5.3.2).[25−27] The starting structure of lightly doped PEDOT:Tos was built on the basis of heavily doped one by removing one of two Tos in the unit cell and simulated annealed via the ab initio molecular dynamics simulations. It was slowly heated to 370 K during the period of 1.5 ps, equilibrated for 1.5 ps at 370 K, and slowly annealed to 0 K during the 1.5 ps simulation. Throughout the calculations, the convergence criterion of the total energy was set to 10^{-5} eV in the self-consistent field iteration. The cutoff energy for the plane-wave basis set was set to 600 eV. The spin−polarization was not considered. The cutoff radius for pair interactions was set to be 50 Å. The Monkhorst−Pack **k**-mesh of 1 × 2 × 2 was used during the simulated annealing and that of 2 × 4 × 4 used during the optimization. The single-point energy and charge density calculations were performed on the **k**-mesh of 4 × 8 × 8. The charge transfer between the host, PEDOT and the dopant, Tos in doped PEDOT:Tos was analyzed with the Bader charge analysis code developed by Henkelman group.[28]

2.2. Transport Property Calculations. The Boltzmann transport theory in the relaxation time approximation was applied to model the microscopic electrical transport process.[29] By solving the steady-state Boltzmann transport equation in the external fields, such as the electric field or thermal gradient, the electrical transport coefficients including the electrical conductivity σ, the Seebeck coefficient S, and the thermal tensor κ_0 can be expressed as

$$\sigma = e^2 \sum_{\mathbf{k}} \left(-\frac{\partial f_0(\varepsilon_{\mathbf{k}})}{\partial \varepsilon_{\mathbf{k}}} \right) \mathbf{v}_{\mathbf{k}} \mathbf{v}_{\mathbf{k}} \tau_{\mathbf{k}} \tag{1}$$

$$S = \frac{e}{\sigma T} \sum_{\mathbf{k}} \mathbf{v}_{\mathbf{k}} \mathbf{v}_{\mathbf{k}} \tau_{\mathbf{k}} \left(-\frac{\partial f_0(\varepsilon_{\mathbf{k}})}{\partial \varepsilon_{\mathbf{k}}} \right) (\varepsilon_{\mathbf{k}} - \mu) \tag{2}$$

$$\kappa_0 = \sum_{\mathbf{k}} \left(-\frac{\partial f_0(\varepsilon_{\mathbf{k}})}{\partial \varepsilon_{\mathbf{k}}} \right) \frac{(\varepsilon_{\mathbf{k}} - \mu)^2}{T} \mathbf{v}_{\mathbf{k}} \mathbf{v}_{\mathbf{k}} \tau_{\mathbf{k}} \tag{3}$$

where $f_0(\varepsilon_{\mathbf{k}}) = 1/(e^{(\varepsilon_{\mathbf{k}} - \mu)/k_B T} + 1)$ is the Fermi−Dirac distribution function, $\mathbf{v}_{\mathbf{k}} = \nabla_{\mathbf{k}} \varepsilon_{\mathbf{k}}/\hbar$ is the group velocity of a charge carrier in a specified band, $\varepsilon_{\mathbf{k}}$ is the band energy at a given **k**-point, μ is the Fermi level. The electronic thermal conductivity can be expressed as

$$\kappa_e = \kappa_0 - S^2 \sigma T \tag{4}$$

The group velocity can be derived from the first-principles band structure calculations. The band energies on a fine Monkhorst−Pack **k**-mesh of 11 × 41 × 41 were calculated for both pristine PEDOT and doped PEDOT:Tos crystals, and interpolated onto a mesh 5 times denser with the smoothed Fourier interpolation method proposed by Madsen and Singh.[30] All the electrical transport coefficients are then derived by evaluating the transport distribution function $\Sigma_{\mathbf{k}} \mathbf{v}_{\mathbf{k}} \mathbf{v}_{\mathbf{k}} \tau_{\mathbf{k}}$, where $\tau_{\mathbf{k}}$ is the relaxation time and a measure of how quickly the charge carriers restore their equilibrium distribution via scatterings with acoustic and optical phonons, impurities or defects. The acoustic phonon scattering was considered in pristine PEDOT. In doped PEDOT:Tos, the ionized impurity scattering with the counterions was included in addition to the acoustic phonon scattering, and by assuming these scatterings are independent, the total relaxation time can be written as $1/\tau = 1/\tau_{ac} + 1/\tau_{imp}$.

The acoustic phonon scattering in both pristine PEDOT and doped PEDOT:Tos was modeled by the deformation potential (DP) theory[31] with the scattering matrix element taking the form $|M(\mathbf{k},\mathbf{k}')|^2 = k_B T E_1^2 / C_{ii}$. Both the elastic constant C_{ii} and deformation potential constant E_1 were derived from first-principles, with details provided in SI. The DP theory has been successfully applied by us to predicting charge carrier mobility of graphene and other carbon allotropes.[32−34] The Brooks−Herring approach was adopted to model the screened Coulomb scattering caused by the ionized counterions in doped PEDOT:Tos. The screened potential takes the form $V(r) = ((q_0 e) e^{-(r/L_D)})/(4\pi\varepsilon\varepsilon_0 r)$, where q_0 is the charge of impurity ions; $L_D = ((\varepsilon\varepsilon_0 k_B T/(e^2 N_0))^{1/2}$ is the Debye screening length; N_0 is the free carrier concentration; ε is the relative permittivity of a material and ε_0 is the dielectric constants of vacuum.[35] The randomly located n scattering centers per unit cell are assumed to scatter independently. The scattering matrix element takes the form of $|M(\mathbf{k},\mathbf{k}')|^2 = (n(q_0 e)^2/(\Omega^2(\varepsilon\varepsilon_0)^2(L_D^{-2} + \mathbf{q}^2)^2)$, where n is the number of dopants per unit cell; $\mathbf{q} = \pm(\mathbf{k}' - \mathbf{k})$ is the scattering wavevector; Ω is the unit cell volume. The relative permittivity of PEDOT was set to be 3.5.[36] The electrical transport coefficients were calculated by the BoltzTraP program,[30,37]

DOI: 10.1021/jacs.5b06584
J. Am. Chem. Soc. 2015, 137, 12929−12938

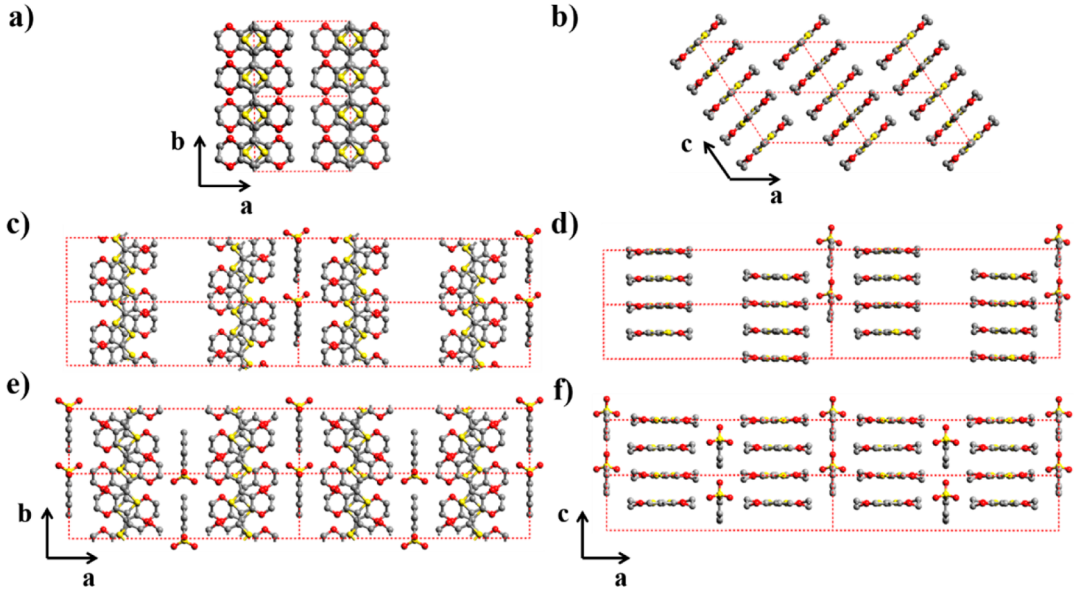

Figure 1. Crystal structures of pristine, lightly, and heavily doped PEDOT crystals. (a,b) *ab* and *ac* planes of pristine PEDOT. (c,d) *ab* and *ac* planes of lightly doped PEDOT. (e,f) *ab* and *ac* planes of heavily doped PEDOT. The red dashed lines represent the crystal lattices. The hydrogen atoms have been removed for the sake of clarity.

in which we incorporated the calculation of relaxation times based on the DP theory and screened Coulomb scattering mechanism.[38−41]

3. RESULTS

The pristine PEDOT is nonconductive or shows very little conductivity, so the oxidant is usually added as a doping agent to improve the conductivity. As a result positive charges are introduced to the backbone of PEDOT and these positive charges are balanced by the counterions provided by the anions of the doping agent. The halides have been previously employed as dopants to increase the polymer conductivity, but their high reactivity and tendency to diffuse may cause serious problems. Other than the halides, organic anions including Tos and PSS, and small molecules such as 2,3,5,6-tetrafluoro-7,7,8,8-tetracyanoquinodimethane (F_4-TCNQ) are frequently used.

3.1. Doping Effect on Backbone and Packing Structures. Each PEDOT monomer contains two EDOT moieties with two sulfur atoms arranging in the *trans*-conformation in a plane (Figure S1). According to the experimental crystal structures of 2,2-bi(3,4-ethylenedioxythiophene) (BEDOT) containing EDOT moieties, the C−C bond of two ethylenedioxy groups in the unit cell of PEDOT was set to be the opposite stereoisomers.[42] The distance between sulfur and oxygen atoms (S···O) is 2.96 Å, which is significantly shorter than the sum of the van der Waals radii of sulfur and oxygen atoms (3.25 Å).[42] This intrachain nonbonded interaction can help to maintain the planar polymer backbone. The distance of S···O in lightly and heavily doped PEDOT:Tos is 2.91 and 2.89 Å respectively, shorter than that in pristine PEDOT, suggesting the stronger S···O nonbonded interactions in doped PEDOT:Tos, which indicates addition of the counterions can increase the planarity of PEDOT backbone. The C−C bond lengths along the conjugated backbone vary in an alternating pattern (Figure S2), and with an increase in the doping level the PEDOT backbone exhibits a transition from aromatic to quinoid-like structure, as identified in the previous calculation of Jean-Luc Brédas et al.[18]

The initial crystal model of PEDOT:Tos was constructed based on the X-ray diffraction by K. E. Aasmundtveit et al.[43] They proposed that in doped PEDOT:Tos, the lamellar structure of pristine PEDOT crystal is retained with the Tos ions locating between the adjacent PEDOT stacks, and forming monolayers,[43] which has also been proved by the experimental structures of PF_6 doped PEDOT,[44] ClO_4^- doped alkyl-substituted PEDOT,[45] trifluoromethanesulfonate (OTF) doped PEDOT, and so on.[46] Recently, Lee et al. proposed that PEDOT:PSS also prefers a lamellar stacking between two alternate PEDOT and PSS layers via X-ray diffraction analysis.[47]

The orientation of the Tos ions within the monolayer was determined by the calculation of Jean-Luc Brédas et al.[18] In their published model of heavily doped PEDOT:Tos the experimental unit cell size was doubled in the direction perpendicular to the Tos layer and only the cell length in the direction of backbone was optimized by using the BLYP functional. In the current investigation, we started from their crystal model of pristine PEDOT and heavily doped PEDOT:Tos, and optimized both the lattice parameters and ionic positions by using the PBE-D functional including the long-range dispersion correction, which is believed to be significant where noncovalent interactions are present. The optimized lattice parameters are provided in Table S1 and comparison with the experimental data and the published theoretical model is available.

The pristine PEDOT is monoclinic with the $\pi-\pi$ stacking direction parallel to the *c* crystal axis. In the *ab* plane, the polymer chain extends along the *b* crystal axis and the insulating layer lines along the *a* crystal axis (Figure 1a,b). Both lightly and heavily doped PEDOT:Tos shows a lamellar structure with the polymer layers and Tos layers alternatively lining along the *a* crystal axis in an orthorhombic unit cell. The distance between adjacent PEDOT layers in lightly doped PEDOT:Tos is larger than heavily doped one due to lack of a monolayer of Tos in the former, because of the stronger charge transfer interactions between PEDOT and Tos as will be

DOI: 10.1021/jacs.5b06584
J. Am. Chem. Soc. 2015, 137, 12929−12938

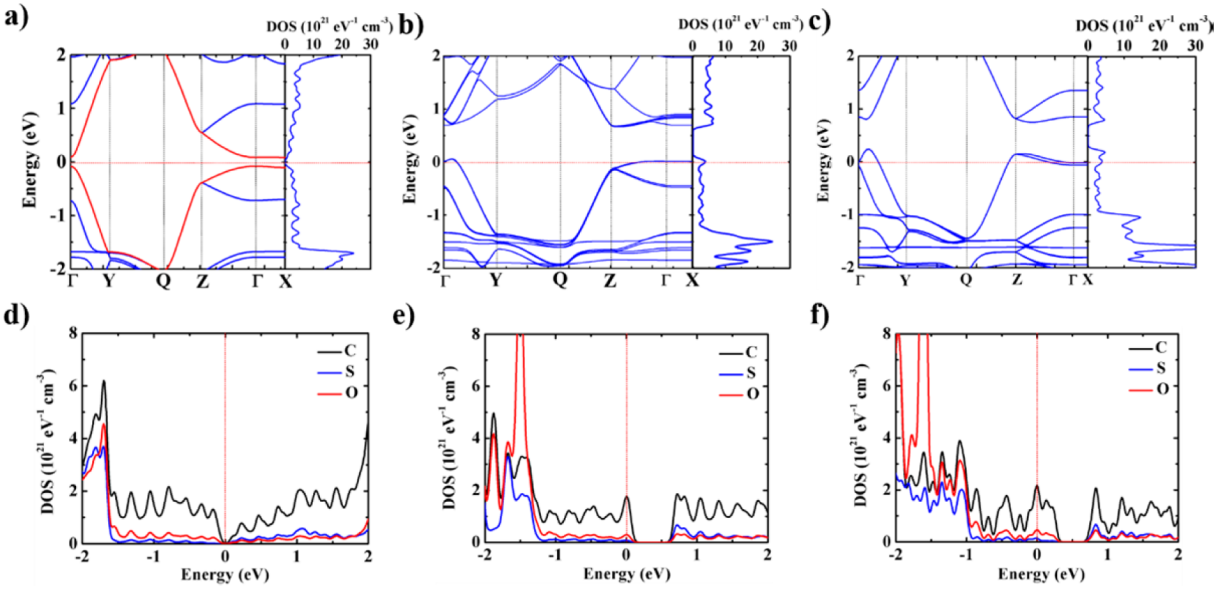

Figure 2. Band structures, DOS, and projected DOS. (a,d) Pristine PEDOT. The highest valence band and lowest conduction band are highlighted in red. (b,e) Lightly doped PEDOT:Tos. (c,f) Heavily doped PEDOT:Tos. The band energies are shifted relative to the Fermi level. The reciprocal coordinates of high-symmetry k-points in the first Brillouin zone are Γ = (0, 0, 0), Y = (0, 0.5, 0), Q = (0, 0.5, 0.5), Z = (0, 0, 0.5) and X = (0.5, 0, 0). The Fermi level is drawn in red dashed line.

discussed below. In the *ac* plane, the $\pi-\pi$ stacking direction is along the *c* crystal axis (Figure 1d,f). The interchain distance in the $\pi-\pi$ stacking direction decreases from 3.52 Å for pristine PEDOT, to 3.37 and 3.36 Å for lightly and heavily doped PEDOT:Tos, which hints on the stronger interactions between conjugated backbones upon addition of Tos. This is due to the formation of quinoid-like structure in doped PEDOT:Tos, making the polymer backbones more rigid and planar than the aromatic structure in pristine PEDOT. It has been evidenced that the benzoid structures prefer coiled configurations, yet the quinoid structures prefer linear or extended configurations.[10] So, the counterions tend to make the PEDOT backbones undergo a transition to the more rigid and planar quinoid structures, which facilitates the formation of more ordered packings between conjugated backbones and increases the crystallinity of conducting polymers.

3.2. Doping Effect on Electronic Structures. The pristine PEDOT is a direct band gap semiconductor with the band gap calculated to be 0.16 eV locating at the Γ-point (Figure 2a). The band gap of nondoped PEDOT films is 1.64 eV measured by vis−NIR absorption spectra,[48] which is much larger than our prediction based on the PBE-D functional, due to the deficiency of DFT in the band gap calculation. The band gap predicted with the hybrid functional HSE06 is 0.53 eV, still far below the experimental result. From the projected density of states (PDOS) analysis (Figure 2d), we find that the oxygen atoms in the ethylenedioxy contribute to both HOMO and LUMO, leading to a charge delocalization, which is a clear evidence for the participation of oxygen atoms in the backbone conjugation. In contrast, the sulfur atoms only contribute to LUMO. Moreover, the band structure of pristine PEDOT exhibits strong anisotropy: the bandwidths of both conduction band (CB) and valence band (VB) along the ΓY direction (1.82 and 1.60 eV respectively) are 4 times larger than those along the ΓZ direction (0.46 eV for CB and 0.30 eV for VB); and the bandwidths of both CB and VB are zero along the ΓX direction. Such feature of band structure is a result of its lamellar structure, and suggests two-dimensional charge transport in pristine PEDOT.

It is evident that for the two doped PEDOT:Tos, the Fermi levels have shifted into the VBs (Figure 2b,e and c,f), showing a metallic behavior, which is in accordance with the ultraviolet photoelectron spectroscopy (UPS) measurement conducted by Xavier Crispin et al.[49] Their experimental results indicate that there are π-electron signals at the Fermi level for both PEDOT:Tos and PEDOT:PSS. The metallic band structure explains the dramatic increase in the conductivity observed for doped PEDOT.[50] The hole concentration in lightly and heavily doped PEDOT:Tos is 1.37 × 10^{20} cm^{-3} and 5.77 × 10^{20} cm^{-3} respectively, as obtained from the position of Fermi level according to the expression $N_p = 2\int_{VB} g(\varepsilon)[1 - f_0(T,\varepsilon,\mu)]\, d\varepsilon$, where $g(\varepsilon)$ is the density of states and $f_0(T,\varepsilon,\mu)$ is the Fermi−Dirac distribution function. Thus, we estimate the doping efficiency, which is defined as the ratio of the density of mobile charge carriers to the density of dopants, to be 20.6% for lightly and 41.5% for heavily doped PEDOT:Tos. It is speculated that the upper limit of doping efficiency of PEDOT:Tos is ∼40% as realized in heavily doped PEDOT:Tos crystal that contains eight EDOT moieties and two Tos counterions per unit cell, since there is no more space to accommodate additional counterions in the unit cell.

The band structures of both lightly and heavily doped PEDOT:Tos are analogous to pristine PEDOT. If removing the flat bands in the energy range between −1.0 eV and −2.0 eV, which are contributed by Tos and lead to sharp peaks in the density of states, the valence band structure resembles that of pristine PEDOT. The relative contribution of C, S, and O elements to the density of states at the position of Fermi level is largely the same in lightly and heavily doped PEDOT:Tos, and it is also close to that at the valence band edge in pristine PEDOT. The derivative of density of states at the position of Fermi level is related to the Seebeck coefficient. Since the position of Fermi level in heavily doped PEDOT:Tos has shifted deep inside the valence band, the Seebeck coefficient

DOI: 10.1021/jacs.5b06584
J. Am. Chem. Soc. 2015, 137, 12929−12938

substantially decreases as will be seen below. The valence band dispersion along the ΓY, namely, the conjugated backbone direction is 1.42 eV for lightly doped and 1.26 eV for heavily doped PEDOT crystals, and that along the ΓZ, namely, the $\pi-\pi$ stacking direction is 0.12 and 0.16 eV respectively. The bandwidths of doped PEDOT:Tos are smaller than those of pristine PEDOT (1.60 eV along the ΓY and 0.30 eV along the ΓZ directions), which is caused by the structural difference between pristine PEDOT and doped PEDOT:Tos. The pristine PEDOT adopts a face-to-face stacking between thiophene rings (Figure 1a) which maximizes the electronic coupling, but doped PEDOT:Tos adopts a face-to-face stacking with a shift of about half thiophene ring along the conjugated backbone (Figure 1c,e), which decreases the electronic coupling. As a result, despite the $\pi-\pi$ stacking distance of doped PEDOT:Tos is smaller than pristine PEDOT as shown above, the band dispersion in that direction decreases because the electronic coupling is determined not only by the stacking distance but also by the nodal structure of frontier orbitals and their relative positions in space. The bandwidth along the backbone direction is smaller in doped PEDOT:Tos because the positive charge located on the thiophene rings induced by doping makes the electron less delocalized.

A critical electronic process of molecular doping is charge transfer between the dopants and the host molecules, which generates sufficient free charge carriers to participate in the transport under the external field. If not taking into account the recombination and dissociation processes of charge carriers, high amount of charge transfer usually gives rise to high doping efficiency. Unfortunately, it has been proved difficult to achieve high doping efficiency for organic semiconductors practically. First, the intermolecular geometrical configuration between the host organic semiconductors and the dopants plays a crucial role to the doping efficiency, such as in D−A copolymers, dopants like F_4-TCNQ located in the vicinity of the acceptor units contribute little to charge transfer.[51,52] Second, it has been shown that in the case of p-doping the frontier orbital hybridization between HOMO of organic semiconductors and LUMO of dopants, leads to the formation of a ground-state charge-transfer complex with reduced energy gap between a doubly occupied bonding and an unoccupied antibonding hybrid orbital. Occupation of all available states follows the Fermi−Dirac statistics. To achieve high doping efficiencies, it demands reduced intermolecular resonance integral in addition to increased electron affinity of dopants.[14,16]

The UV−vis or NIR spectroscopy and X-ray photoelectronic spectroscopy (XPS) are common methods to infer the doping levels. In the case of PEDOT, the doping occurs during the polymerization and Tos act as counterions instead of oxidants. In our chemical model, number of Tos included in each unit cell indicates the level of doping. Here, we estimate the amount of charge transfer between PEDOT and Tos with the assistance of Bader's population analysis.[28] By analyzing the atomic charges in lightly and heavily doped PEDOT:Tos labeled in Figure 3, we can estimate that 0.89 and 0.87 electrons are transferred from PEDOT to each Tos for lightly and heavily doped PEDOT:Tos, respectively. By comparing the atomic charges in doped PEDOT:Tos with those in pristine PEDOT and isolated Tos, we conclude that the major electron donating atoms are carbon atoms bonded to the ethylenedioxy groups and sulfur atoms in the thiophene rings, and the electron acceptors are mainly located on the three oxygen atoms of Tos (Figure 3a−c). Previous theoretical work has demonstrated that

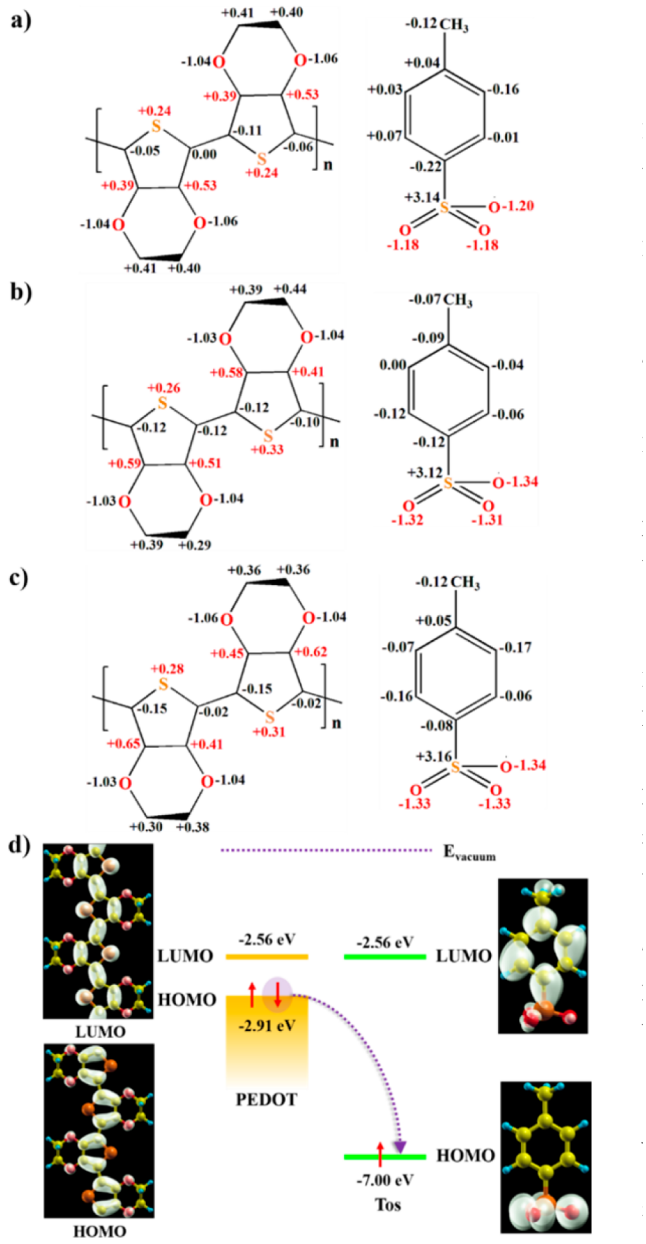

Figure 3. Atomic charge analysis and a schematic illustration of charge transfer in doped PEDOT:Tos. (a) Pristine PEDOT and isolated Tos. (b) Lightly doped PEDOT:Tos. (c) Heavily doped PEDOT:Tos. (d) Energy level diagrams of undoped PEDOT and isolated Tos as well as their frontier orbitals. The atomic charges of hydrogen are not shown for the sake of clarity.

the amount of charge transfer from oligothiophene derivatives to F_4-TCNQ falls into the range betwen 0.4 and 0.7 electrons according to the natural orbital population analysis.[17] Compared to that, the amount of charge transfer from PEDOT to Tos is close to unity, so the doping efficiency of PEDOT:Tos should be higher. The different exchange-correlation functionals including PBE-D, LDA and PBE, have been tested, and we find negligible influence of the choice of functionals on the amount of charge transfer (Table S4).

The absolute energy levels of frontier orbitals of undoped PEDOT and isolated Tos, with respect to the vacuum energy level are obtained, and the charge transfer process is schematically illustrated in Figure 3d. The vacuum level

DOI: 10.1021/jacs.5b06584
J. Am. Chem. Soc. 2015, 137, 12929−12938

calibration method has been demonstrated in Figure S3. As can be seen from the energy level diagrams of PEDOT and Tos, the HOMO of Tos is below that of PEDOT and singly occupied with electron density located on oxygen atoms. There is barely no electron density on oxygen atoms in the LUMO of Tos. We infer that a charge transfer occurs from the HOMO of host polymer to the HOMO of Tos, since we see in the above atomic charge analysis the electron acceptors of the charge transfer process are the oxygen atoms of Tos. The close-to-unity charge transfer from PEDOT to Tos is consistent with the known fact that the Tos act as counterions in the oxidation and polymerization of EDOT.

3.3. Doping Effect on Transport Properties. We derived the TE transport properties based on the Boltzmann transport equation and the relaxation time approximation.[29] For pristine PEDOT, we include only the acoustic phonon scattering of charge carriers. Since PEDOT is a p-type semiconducting polymer, we focus on the hole transport in the following. Within the rigid band approximation, the Seebeck coefficient and electrical conductivity are obtained as a function of charge carrier concentration by varying the position of Fermi level. As shown in Figure 4, the Seebeck coefficient decreases linearly

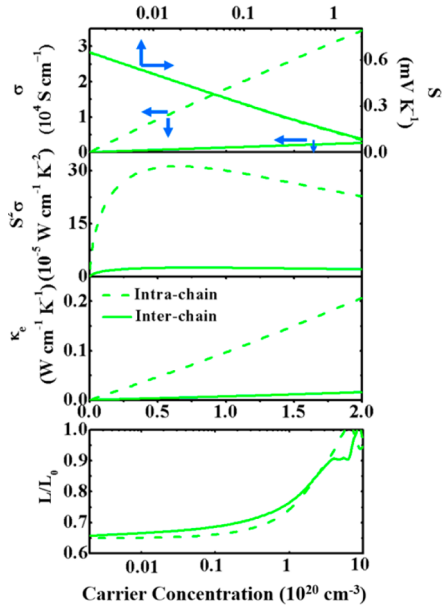

Figure 4. Electrical conductivity, Seebeck coefficient, TE power factor, electronic thermal conductivity and relative Lorenz number of pristine PEDOT, as a function of the hole concentration at 298 K. The relaxation times are computed based on the DP theory. The Seebeck coefficient and relative Lorenz number are plotted versus the logarithm of the hole concentration. The intrachain direction represents the backbone direction along the crystal axis *b*, and the interchain direction represents the stacking direction along the crystal axis *c*.

with the logarithm of the carrier concentration, whereas the electrical conductivity increases linearly with the carrier concentration at low carrier concentrations. Consequently, a maximum of power factor $S^2\sigma$ is achieved at certain carrier concentration denoted as the optimal doping level. The corresponding electrical transport coefficients at the optimal doping level have been included in Table 1. The electronic thermal conductivity also increases linearly with the carrier concentration, and a linear relation between the electronic thermal conductivity and the electrical conductivity holds, $\kappa_e = L\sigma T$, which is known as the Wiedemann–Franz law. For free-electron gas, the Lorenz number is the theoretical Sommerfeld value $L_0 = (\pi^2/3)(k_B/e)^2$. The calculated Lorentz number is lower than the Sommerfeld value at low carrier concentrations, such as in the case of lightly doped PEDOT:Tos, and it approaches the theoretical Sommerfeld value at high carrier concentrations where a semiconductor-to-metal transition occurs, such as in the case of heavily doped PEDOT:Tos. Our observation is in agreement with a recent measurement of thermal conductivity of drop-cast PEDOT:PSS films, in which the increase in thermal conductivity as a function of electrical conductivity can be related to the electronic component of thermal conductivity by applying the Wiedemann–Franz law with conventional Sommerfeld value of the Lorenz number.[53] It indicates that the calculated electronic thermal conductivities are close to those experimentally derived values at the same electrical conductivities. In another measurement, thermal conductivity of the PEDOT:Tos samples was found to increase with the electrical conductivity, and the increase exceeds that predicted by the Wiedemann–Franz law based on the Sommerfeld value of the Lorenz number.[11] They ascribed the larger Lorenz number to both phonon-assisted hopping and a bipolar contribution in the disordered barrier regions of PEDOT.[11] It should be mentioned that the theoretical model used by us is based on an ideal crystal and delocalized band transport, and a more elaborate transport model incorporating charge localization effect could be considered in the future.

A linear relationship between the Seebeck coefficient and the logarithm of the electrical conductivity shows up (Figure 5a). As illustrated in an earlier work of us,[41] this simple relation can be easily derived by assuming that the carrier concentration is low and the carriers only transport in one band

$$S = -\frac{k_B}{e}\ln\sigma_p + \frac{k_B}{e}\ln(N_{eff}e\mu_p) \quad (5)$$

The above equation indicates that the slope of the S–$\ln\sigma$ curve $-k_B/e$ is determined by two elementary constants, the Boltzmann constant k_B and the elementary charge e. The intercept $(k_B/e)\ln(N_{eff}e\mu_p)$ is related to the effective density of states N_{eff} and the charge carrier mobility μ. The experimental results of PEDOT TE properties have been plotted in Figure 5a for comparison. In the experiments, PEDOT is often doped with PSS or Tos. An early research reported a relatively low and nonoptimized zT value around 1.75×10^{-3} for PEDOT:PSS.[10] By replacing the counterions PSS with smaller Tos to prevent generation of insulating phase with polyanions, and by accurately controlling the oxidation level via step by step reduction, the zT value was optimized to 0.25.[8] In a parallel experiment, large power factors of 12.7 μW cm^{-1} K^{-2} has been achieved for PEDOT:Tos films by the precise control of the oxidation level via the electrochemical approach.[54] The measured Seebeck coefficients and the logarithm of conductivities indeed display a well-defined linear relationship with a uniform slope equal to $-k_B/e$. It has also been shown that minimizing the total volume of dopants by removing the nonionized dopant species from PEDOT:PSS can improve the TE figure of merit,[9] because the nonionized dopants in PEDOT:PSS can significantly alter the configuration of conducting hosts, reduce the carrier mobility and TE power factor. These state-of-the-art experiments all stress the importance of doping optimization in the improvement of TE efficiencies. Because the available experimental data for

DOI: 10.1021/jacs.5b06584
J. Am. Chem. Soc. 2015, 137, 12929–12938

Table 1. TE Transport Properties of Pristine PEDOT at the Optimal Doping Level and Two Explicitly Doped PEDOT:Tos, Compared with Available Experimental Results

	directions	carrier concentration (10^{20} cm^{-3})	S (mV K^{-1})	σ (10^3 S cm^{-1})	$S^2\sigma$ (μW cm^{-1} K^{-2})	κ_e (W cm^{-1} K^{-1})	μ (cm^2 V^{-1} s^{-1})	L/L_0
pristine	*b*	0.65	0.16	12.0	312	0.06	1.25×10^3	0.71
	c	0.77	0.15	1.05	24.8	0.006	94.5	0.75
lightly doped	*b*	1.37	0.13	1.95	31.5	0.01	89.0	0.77
	c		0.11	0.16	2.09	0.0008	7.28	0.66
heavily doped	*b*	5.77	0.01	92.6	9.21	0.68	1.00×10^3	1.00
	c		0.005	12.1	0.31	0.08	131	0.93
PEDOT:Tos[8]			0.22	0.08	3.50			
PEDOT:PSS[9]			0.07	0.90	4.50			
PEDOT:Tos[54]			0.12	0.92	12.7			

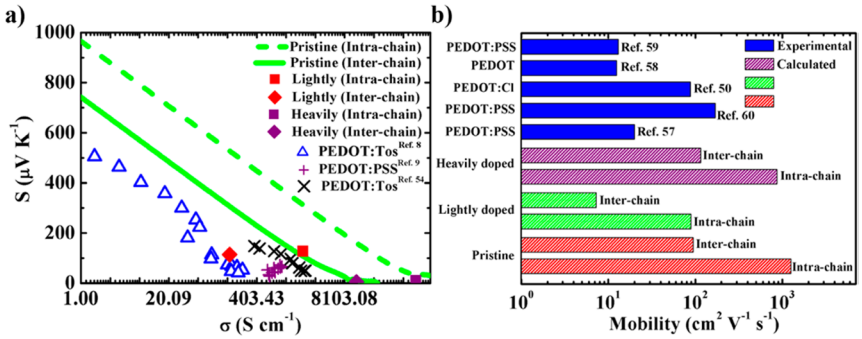

Figure 5. Mobility, electrical conductivity, and Seebeck, a comparison between theory and experiments. (a) Seebeck coefficient and logarithm of electrical conductivity relationship. (b) Predicted and measured mobilities of PEDOT.

PEDOT:PSS span a narrow range of carrier concentrations, we cannot unambiguously identify the slope between the Seebeck and the logarithm of conductivity. We noticed that all the experimental data distribute below the theoretical line, with the intercept smaller than the prediction, which according to eq 5 indicates that the carrier mobility calculated within the rigid band approximation and including merely the acoustic phonon scattering has been overestimated due to the neglection of the explicit doping effect.

In fact, all the earlier investigations of the TE transport has adopted the rigid band approximation, without explicitly accounting for the doping effect. In this approximation, the doping effect is mimicked by shifting the chemical potential in the Fermi–Dirac distribution function and assuming band structures of conducting molecules remain unchanged in the process of doping. This approximation is usually valid at low carrier concentrations, but the effect of doping on the TE transport cannot be explicitly included. In the above we have demonstrated the doping effect on the geometry and electronic structure of PEDOT. In the following we explore explicitly the doping effect on the charge and TE transport properties of PEDOT. In doped PEDOT:Tos the Tos are partially ionized and they can scatter charge carriers via screened Coulomb interactions, in analogy to the ionized impurity scattering mechanism. In addition, inclusion of the counterions in the host matrix also altered the phonon scattering effect, mainly because different packing structures between pristine PEDOT and doped PEDOT:Tos, with intercalation of the counterions in the latter, lead to different elastic constants. To obtain the total relaxation time of charge carriers, we assume that the two scattering mechanisms are independent of each other and Matthiessen's rule can be applied. The dopant scattering probability is proportional to its concentration, which is 6.65×10^{20} cm^{-3} for lightly and 1.39×10^{21} cm^{-3} for heavily doped PEDOT:Tos. The effective charge of Tos acting as ionized scattering center is taken to be 0.89 for lightly and 0.87 for heavily doped PEDOT:Tos. We find that the ionized impurity scattering dominates over the acoustic phonon scattering over the temperature range between 10 and 300 K (Figure S5). A quantitative comparison of electron–phonon and impurity scatterings based on the first-principles calculations has been made possible in silicon. The overall mobility calculated agrees well with the experimental values at room temperature and they found that the impurity scattering is dominant at carrier concentrations larger than 10^{17} cm^{-3}.[55] Gleason et al. have studied charge transport in heavily doped PEDOT with Cl^- as counterions at the carrier concentration higher than 10^{20} cm^{-3}. By comparing the Hall measurement and the theoretical calculation, they demonstrated that the charge transport process in PEDOT:Cl is governed by the ionized impurity scattering mechanism.[56] The relaxation times due to ionized impurity scattering and acoustic phonon scattering both exhibit a power law temperature dependence, with the former decreasing faster with the temperature (Figure S5).

After including both acoustic phonon scattering and ionized dopant scattering effects in the explicitly doped PEDOT:Tos, charge carrier mobility in lightly doped PEDOT:Tos is lowered by at least 1 order of magnitude, while that in heavily doped PEDOT:Tos remains largely unchanged. The reason is that the carrier concentration in heavily doped PEDOT:Tos is high, which results in strong Coulomb screening effect and weak scattering of charge carriers with the counterions. The acoustic phonon scattering in doped PEDOT:Tos is also weaker than pristine PEDOT, mainly because the elastic constant in doped PEDOT:Tos is significantly larger along the crystal axis *a* due to the insertion of Tos (Table S6). The Seebeck-conductivity

DOI: 10.1021/jacs.5b06584
J. Am. Chem. Soc. 2015, 137, 12929–12938

data of lightly doped PEDOT:Tos lies right above the experimental lines of PEDOT:Tos in Figure 5a, with that along the backbone direction close to the experimental values reported in ref 54 via electrochemical control of the oxidation level, and the one along the stacking direction close to the experimental values reported in ref 8. The Seebeck-conductivity data of heavily doped PEDOT:Tos locates on the line predicted within the rigid band approximation, because the charge carrier mobility, as mentioned above, remains roughly unchanged upon heavy doping.

The electrical transport coefficients of lightly and heavily doped PEDOT:Tos are collected in Table 1, in comparison with the available experimental data at the optimal oxidation level. As can be seen from Table 1, with the carrier concentration increasing from 1.37×10^{20} to 5.77×10^{20} cm^{-3}, the Seebeck coefficient decreases dramatically, while the electrical conductivity and electronic thermal conductivity increase. This behavior has been predicted within the rigid band approximation. The power factor of heavily doped PEDOT:Tos is much lower than lightly doped PEDOT:Tos. Apparently, the heavily doped PEDOT:Tos is over doped, and its counterion concentration is twice that of lightly doped one, showing that the doping control for maximized TE efficiency is delicate and challenging. The power factor of lightly doped PEDOT:Tos is 31.5 $\mu W\ cm^{-1}\ K^{-2}$ along the crystal axis *b* and 2.09 $\mu W\ cm^{-1}\ K^{-2}$ along the crystal axis *c*, which compared reasonably well with the experimental values of 12.7 $\mu W\ cm^{-1}\ K^{-2}$ reported by Eunkyoung Kim[54] and 3.5 $\mu W\ cm^{-1}\ K^{-2}$ reported by Xavier Crispin.[8]

The experimental measurements were conducted on the PEDOT thin films, while our calculations are based on the ordered crystals. We noticed that the charge and TE transport in the PEDOT crystal is highly anisotropic, with the conductivity and power factor along the backbone direction 1 order of magnitude larger than those along the stacking direction. The Seebeck coefficient is however isotropic, since it is a measure of the charge carrier movement driven by heat and represents the entropy per unit charge carried by the electric current. As seen from eq 2, the Seebeck coefficient can be expressed as a ratio of two transport tensors. Both of them are anisotropic due to the anisotropic group velocity and band structures. The anisotropy of the two tensors is to some extent canceled out, leading to the isotropic Seebeck coefficient. The TE figure of merit relies on the electrical transport coefficients as well as the lattice thermal conductivity. The thermal transport is also anisotropic, and the electronic thermal conductivity in lightly doped PEDOT:Tos is usually trivial compared to the lattice thermal conductivity, in either direction. To improve the TE efficiency, we should resolve to utilize the high power factor along the backbone direction and the low lattice thermal conductivity along the stacking and insulating directions.

The charge carrier mobility is a charge transport property of great importance, and it relates to the TE transport property via the conductivity through the relation $\sigma = \mu eN$. We have pointed out in an earlier publication that a high intrinsic mobility usually leads to a high TE figure of merit at the optimal doping level.[41] The predicted mobilities in both lightly and heavily doped PEDOT:Tos are provided in Table 1, and summarized in Figure 5b together with experimentally reported mobilities for PEDOT.[50,57−60] Overall, our predictions agree reasonably well with the experimental values. Especially, a high hole conductivity of 8797 S cm^{-1} and mobility of 88.08 $cm^2\ V^{-1}\ s^{-1}$ at the doping level of 6.23×10^{20} cm^{-3} have been observed in single crystal PEDOT nanowires in the direction of $\pi-\pi$ stacking with Cl^- counter-anions,[50] which is close to the predicted values of 1.21×10^4 S cm^{-1} and 131 $cm^2\ V^{-1}\ s^{-1}$ at the carrier concentration of 5.77×10^{20} cm^{-3} in heavily doped PEDOT:Tos. It is also noticed that the mobility is highly anisotropic, with the intrachain mobility along the backbone direction 1 order of magnitude larger than the interchain mobility along the stacking direction. In practice, polymers are often characterized by amorphous structures, poor packing configurations, and low degree of polymerization, which lead to low charge carrier mobilities. Nevertheless, with improved fabrication techniques, such as to increase the crystallinity, the recently reported charge carrier mobilities for conducting polymers are much higher than before, easily exceeding 10 $cm^2\ V^{-1}\ s^{-1}$.[19,21] For instance, an ultrahigh intrinsic hole mobility of 71 $cm^2\ V^{-1}\ s^{-1}$ was reported for the highly oriented nanocrystal of poly[4-(4,4-dihexadecyl-4*H*-cyclopenta[1,2-b:5,4-b′]-dithiophen-2-yl)-*alt*-[1,2,5]-thiadiazolo[3,4-*c*]pyridine] (PCDTPT) in the direction of chain alignment according to Heeger et al.[22] Their work also manifests a strong anisotropy of charge transport, with mobility in the direction of chain alignment at least 10-fold higher than that in the perpendicular direction, which is in accordance with our theoretical prediction for PEDOT. We believe that a large majority of mobilities experimentally reported are low because the samples are amorphous, adopting coiled configurations with chain entanglements and folding. The high mobility of conducting polymers could be acquired once the crystallinity is improved, such as by changing the size of counterions,[61] and by adding polar solvent to water dispersion before film preparation or post-treating the samples in the polar solvent.[62,63] It has been demonstrated that some conjugated polymers such as indacenodithiophene-*co*-benzothiadiazole (IDTBT) with less crystalline microstructures than crystalline or semicrystalline, also exhibit high field-effect mobilities.[24] The role of long polymer chains connecting the crystalline domains and promoting high mobility in polycrystalline samples of semiconducting polymers, has been reported.[20] The enhanced mobility should be of benefit to the improvement of power factors of conducting polymers.

4. DISCUSSION

PEDOT is one of the best organic materials reported so far for TE applications. The accurate doping control has been demonstrated as the most successful strategy to enhance its energy conversion efficiency. The counterions commonly used include PSS, Tos, and halides. The TE figure of merit for optimized PEDOT:PSS has been demonstrated to be 2 orders of magnitude higher than the nonoptimized one. Compared to polyanions, it is easy to control the amount of small-sized anions, yet small anions tend to diffuse and such doped polymers may suffer from stability issues. In addition, the counterions especially polyanions may change the configurations of host polymers, and influence their charge transport properties. In an earlier investigation, we proposed to search for organic TE materials with high mobilities, because high mobility usually leads to high figure of merit and requires low level of doping. It has been believed that organic semiconductors and conjugated polymers are often characterized by structural disorder due to their soft nature and weak van der Waals interactions, and their mobilities are much lower than inorganic semiconductors. However, recent experimental

DOI: 10.1021/jacs.5b06584
J. Am. Chem. Soc. 2015, 137, 12929−12938

advances demonstrated that by improving fabrication methods and controlling the morphology, high charge carrier mobility in the range of 10−20 cm^2 V^{-1} s^{-1} can be easily achieved in conjugated polymers including PEDOT. The high mobility should be of benefit to the improvement of TE properties of conducting polymers. In this work we investigated the doping effect on the charge and TE transport in PEDOT, by inclusion of Tos in the chemical model and explicitly taking into account their scattering to the charge carriers. The predicted mobility and power factors are in very good agreement with the state-of-the-art experimental data. We believe that by an appropriate control of the doping level, it is viable to attain comparable TE performance in conjugated polymers with high mobilities other than PEDOT.

The other key element influencing the TE figure of merit of a material is the lattice thermal conductivity, which deserves some discussion. It has been suggested that the electrical transport properties and the lattice thermal conductivity can be optimized separately. Similar to charge and TE transport in highly ordered systems, thermal transport arising from the lattice vibrations is anisotropic too. Our preliminary calculations of the lattice thermal conductivity in pristine PEDOT suggest a thermal conductivity in the direction of backbone 2 orders of magnitude higher than the direction of stacking. As a result, a higher TE figure of merit is expected in the direction of stacking, although a higher power factor is obtained in the direction of backbone. To further enhance the TE efficiency, we propose to utilize the high power factor in the direction of polymer backbone, and the low lattice thermal conductivity in the other two directions. Recently, thermal conductivity of polymers as an important material property has drawn serious attention. Engineering thermal conductivity by drawing polymeric fibres[64] or changing interchain interactions has been reported.[65] Interestingly, enhanced thermal conductivity is discovered in polythiophene nanofibres due to significant molecular chain orientation along the fiber axis, but the dominant phonon scattering process is still related to structural disorder.[66] For the improved TE figure of merit, both increased chain alignment and some sort of structural disorder are desired, and such features are anticipated in amorphous polymers with high mobility,[24] polycrystalline polymers with long polymer chains connecting the crystalline domains,[20] or chain-oriented amorphous polymeric nanofibres.[66]

■ ASSOCIATED CONTENT

Supporting Information

The Supporting Information is available free of charge on the ACS Publications website at DOI: 10.1021/jacs.5b06584.

Supplementary figures and tables, computational details and supplementary references. (PDF)

■ AUTHOR INFORMATION

Corresponding Authors

*dong913@tsinghua.edu.cn

*zgshuai@tsinghua.edu.cn

Notes

The authors declare no competing financial interest.

■ ACKNOWLEDGMENTS

This work is supported by the National Natural Science Foundation of China (Grant nos. 21273124, 21290190, and 91333202) and the Ministry of Science and Technology of China (Grant no. 2013CB933503). Computational resources are provided by the Tsinghua Supercomputing Center.

■ REFERENCES

(1) DiSalvo, F. J. *Science* **1999**, *285*, 703.
(2) Bell, L. E. *Science* **2008**, *321*, 1457.
(3) Zhang, Q.; Sun, Y.; Xu, W.; Zhu, D. *Adv. Mater.* **2014**, *26*, 6829.
(4) Chen, Y.; Zhao, Y.; Liang, Z. *Energy Environ. Sci.* **2015**, *8*, 401.
(5) McGrail, B. T.; Sehirlioglu, A.; Pentzer, E. *Angew. Chem., Int. Ed.* **2015**, *54*, 1710.
(6) Mai, C.-K.; Schlitz, R. A.; Su, G. M.; Spitzer, D.; Wang, X.; Fronk, S. L.; Cahill, D. G.; Chabinyc, M. L.; Bazan, G. C. *J. Am. Chem. Soc.* **2014**, *136*, 13478.
(7) Shi, K.; Zhang, F.; Di, C.-A.; Yan, T.-W.; Zou, Y.; Zhou, X.; Zhu, D.; Wang, J.-Y.; Pei, J. *J. Am. Chem. Soc.* **2015**, *137*, 6979.
(8) Bubnova, O.; Khan, Z. U.; Malti, A.; Braun, S.; Fahlman, M.; Berggren, M.; Crispin, X. *Nat. Mater.* **2011**, *10*, 429.
(9) Kim, G. H.; Shao, L.; Zhang, K.; Pipe, K. P. *Nat. Mater.* **2013**, *12*, 719.
(10) Jiang, F. X.; Xu, J. K.; Lu, B. Y.; Xie, Y.; Huang, R. J.; Li, L. F. *Chin. Phys. Lett.* **2008**, *25*, 2202.
(11) Weathers, A.; Khan, Z. U.; Brooke, R.; Evans, D.; Pettes, M. T.; Andreasen, J. W.; Crispin, X.; Shi, L. *Adv. Mater.* **2015**, *27*, 2101.
(12) Reenen, S. v.; Kemerink, M. *Org. Electron.* **2014**, *15*, 2250.
(13) Bubnova, O.; Berggren, M.; Crispin, X. *J. Am. Chem. Soc.* **2012**, *134*, 16456.
(14) Salzmann, I.; Heimel, G.; Duhm, S.; Oehzelt, M.; Pingel, P.; George, B. M.; Schnegg, A.; Lips, K.; Blum, R.-P.; Vollmer, A.; Koch, N. *Phys. Rev. Lett.* **2012**, *108*, 035502.
(15) Hansson, A.; Böhlin, J.; Stafström, S. *Phys. Rev. B: Condens. Matter Mater. Phys.* **2006**, *73*, 184114.
(16) Méndez, H.; Heimel, G.; Opitz, A.; Sauer, K.; Barkowski, P.; Oehzelt, M.; Soeda, J.; Okamoto, T.; Takeya, J.; Arlin, J.-B.; Balandier, J.-Y.; Geerts, Y.; Koch, N.; Salzmann, I. *Angew. Chem., Int. Ed.* **2013**, *52*, 7751.
(17) Zhu, L.; Kim, E.-G.; Yi, Y.; Brédas, J.-L. *Chem. Mater.* **2011**, *23*, 5149.
(18) Kim, E.-G.; Brédas, J.-L. *J. Am. Chem. Soc.* **2008**, *130*, 16880.
(19) Kang, I.; Yun, H.-J.; Chung, D. S.; Kwon, S.-K.; Kim, Y.-H. *J. Am. Chem. Soc.* **2013**, *135*, 14896.
(20) Noriega, R.; Rivnay, J.; Vandewal, K.; Koch, F. P. V.; Stingelin, N.; Smith, P.; Toney, M. F.; Salleo, A. *Nat. Mater.* **2013**, *12*, 1038.
(21) Kim, G.; Kang, S.-J.; Dutta, G. K.; Han, Y.-K.; Shin, T. J.; Noh, Y.-Y.; Yang, C. *J. Am. Chem. Soc.* **2014**, *136*, 9477.
(22) Luo, C.; Kyaw, A. K. K.; Perez, L. A.; Patel, S.; Wang, M.; Grimm, B.; Bazan, G. C.; Kramer, E. J.; Heeger, A. J. *Nano Lett.* **2014**, *14*, 2764.
(23) Tseng, H.-R.; Phan, H.; Luo, C.; Wang, M.; Perez, L. A.; Patel, S. N.; Ying, L.; Kramer, E. J.; Nguyen, T.-Q.; Bazan, G. C.; Heeger, A. J. *Adv. Mater.* **2014**, *26*, 2993.
(24) Venkateshvaran, D.; Nikolka, M.; Sadhanala, A.; Lemaur, V.; Zelazny, M.; Kepa, M.; Hurhangee, M.; Kronemeijer, A. J.; Pecunia, V.; Nasrallah, I.; Romanov, I.; Broch, K.; McCulloch, I.; Emin, D.; Olivier, Y.; Cornil, J.; Beljonne, D.; Sirringhaus, H. *Nature* **2014**, *515*, 384.
(25) Blöchl, P. E. *Phys. Rev. B: Condens. Matter Mater. Phys.* **1994**, *50*, 17953.
(26) Kresse, G.; Furthmüller, J. *Phys. Rev. B: Condens. Matter Mater. Phys.* **1996**, *54*, 11169.
(27) Grimme, S. *J. Comput. Chem.* **2006**, *27*, 1787.
(28) Henkelman, G.; Arnaldsson, A.; Jónsson, H. *Comput. Mater. Sci.* **2006**, *36*, 354.
(29) Nag, B. R. *Electron Transport in Compound Semiconductors*; SpringerVerlag: Berlin, 1980.
(30) Madsen, G. K. H. *J. Am. Chem. Soc.* **2006**, *128*, 12140.
(31) Bardeen, J.; Shockley, W. *Phys. Rev.* **1950**, *80*, 72.
(32) Long, M.-Q.; Tang, L.; Wang, D.; Wang, L.; Shuai, Z. *J. Am. Chem. Soc.* **2009**, *131*, 17728.
(33) Long, M.; Tang, L.; Wang, D.; Li, Y.; Shuai, Z. *ACS Nano* **2011**, *5*, 2593.

DOI: 10.1021/jacs.5b06584
J. Am. Chem. Soc. 2015, 137, 12929−12938

(34) Chen, J.; Xi, J.; Wang, D.; Shuai, Z. *J. Phys. Chem. Lett.* **2013**, *4*, 1443.
(35) Chattopadhyay, D.; Queisser, H. J. *Rev. Mod. Phys.* **1981**, *53*, 745.
(36) Abidian, M. R.; Martin, D. C. *Biomaterials* **2008**, *29*, 1273.
(37) Madsen, G. K. H.; Singh, D. J. *Comput. Phys. Commun.* **2006**, *175*, 67.
(38) Chen, J.; Wang, D.; Shuai, Z. *J. Chem. Theory Comput.* **2012**, *8*, 3338.
(39) Wang, D.; Shi, W.; Chen, J.; Xi, J.; Shuai, Z. *Phys. Chem. Chem. Phys.* **2012**, *14*, 16505.
(40) Shuai, Z.; Wang, D.; Peng, Q.; Geng, H. *Acc. Chem. Res.* **2014**, *47*, 3301.
(41) Shi, W.; Chen, J.; Xi, J.; Wang, D.; Shuai, Z. *Chem. Mater.* **2014**, *26*, 2669.
(42) Raimundo, J.-M.; Blanchard, P.; Frère, P.; Mercier, N.; Ledoux-Rak, I.; Hierle, R.; Roncali, J. *Tetrahedron Lett.* **2001**, *42*, 1507.
(43) Aasmundtveit, K. E.; Samuelsen, E. J.; Pettersson, L. A. A.; Inganäs, O.; Johansson, T.; Feidenhans'l, R. *Synth. Met.* **1999**, *101*, 561.
(44) Niu, L.; Kvarnström, C.; Fröberg, K.; Ivaska, A. *Synth. Met.* **2001**, *122*, 425.
(45) Breiby, D. W.; Samuelsen, E. J.; Groenendaal, L. B.; Struth, B. *J. Polym. Sci., Part B: Polym. Phys.* **2003**, *41*, 945.
(46) Massonnet, N.; Carella, A.; de Geyer, A.; Faure-Vincent, J.; Simonato, J.-P. *Chem. Sci.* **2015**, *6*, 412.
(47) Kim, N.; Kee, S.; Lee, S. H.; Lee, B. H.; Kahng, Y. H.; Jo, Y.-R.; Kim, B.-J.; Lee, K. *Adv. Mater.* **2014**, *26*, 2268.
(48) Havinga, E. E.; Mutsaers, C. M. J.; Jenneskens, L. W. *Chem. Mater.* **1996**, *8*, 769.
(49) Bubnova, O.; Khan, Z. U.; Wang, H.; Braun, S.; Evans, D. R.; Fabretto, M.; Hojati-Talemi, P.; Dagnelund, D.; Arlin, J.-B.; Geerts, Y. H.; Desbief, S.; Breiby, D. W.; Andreasen, J. W.; Lazzaroni, R.; Chen, W. M.; Zozoulenko, I.; Fahlman, M.; Murphy, P. J.; Berggren, M.; Crispin, X. *Nat. Mater.* **2014**, *13*, 190.
(50) Cho, B.; Park, K. S.; Baek, J.; Oh, H. S.; Koo Lee, Y.-E.; Sung, M. M. *Nano Lett.* **2014**, *14*, 3321.
(51) Di Nuzzo, D.; Fontanesi, C.; Jones, R.; Allard, S.; Dumsch, I.; Scherf, U.; von Hauff, E.; Schumacher, S.; Da Como, E. *Nat. Commun.* **2015**, *6*, 6460.
(52) Duong, D. T.; Phan, H.; Hanifi, D.; Jo, P. S.; Nguyen, T.-Q.; Salleo, A. *Adv. Mater.* **2014**, *26*, 6069.
(53) Liu, J.; Wang, X.; Li, D.; Coates, N. E.; Segalman, R. A.; Cahill, D. G. *Macromolecules* **2015**, *48*, 585.
(54) Park, T.; Park, C.; Kim, B.; Shin, H.; Kim, E. *Energy Environ. Sci.* **2013**, *6*, 788.
(55) Restrepo, O. D.; Varga, K.; Pantelides, S. T. *Appl. Phys. Lett.* **2009**, *94*, 212103.
(56) Lee, S.; Paine, D. C.; Gleason, K. K. *Adv. Funct. Mater.* **2014**, *24*, 7187.
(57) Ashizawa, S.; Shinohara, Y.; Shindo, H.; Watanabe, Y.; Okuzaki, H. *Synth. Met.* **2005**, *153*, 41.
(58) Taggart, D. K.; Yang, Y.; Kung, S.-C.; McIntire, T. M.; Penner, R. M. *Nano Lett.* **2010**, *11*, 125.
(59) Lin, Y.-J.; Tsai, C.-L.; Su, Y.-C.; Liu, D.-S. *Appl. Phys. Lett.* **2012**, *100*, 253302.
(60) Okuzaki, H.; Ishihara, M.; Ashizawa, S. *Synth. Met.* **2003**, *137*, 947.
(61) Culebras, M.; Gomez, C. M.; Cantarero, A. *J. Mater. Chem. A* **2014**, *2*, 10109.
(62) Takano, T.; Masunaga, H.; Fujiwara, A.; Okuzaki, H.; Sasaki, T. *Macromolecules* **2012**, *45*, 3859.
(63) Wei, Q.; Mukaida, M.; Naitoh, Y.; Ishida, T. *Adv. Mater.* **2013**, *25*, 2831.
(64) Shen, S.; Henry, A.; Tong, J.; Zheng, R.; Chen, G. *Nat. Nanotechnol.* **2010**, *5*, 251.
(65) Kim, G.-H.; Lee, D.; Shanker, A.; Shao, L.; Kwon, M. S.; Gidley, D.; Kim, J.; Pipe, K. P. *Nat. Mater.* **2015**, *14*, 295.
(66) Singh, V.; Bougher, T. L.; Weathers, A.; Cai, Y.; Bi, K.; Pettes, M. T.; McMenamin, S. A.; Lv, W.; Resler, D. P.; Gattuso, T. R.; Altman, D. H.; Sandhage, K. H.; Shi, L.; Henry, A.; Cola, B. A. *Nat. Nanotechnol.* **2014**, *9*, 384.

DOI: 10.1021/jacs.5b06584
J. Am. Chem. Soc. 2015, 137, 12929−12938